Borophene: A piezocatalyst for water remediation

Aditi Sharma, Upasana Bhardwaj, Maya Marinova, Antonio Da Costa, Anthony Ferri, Sebastien Royer, Himmat Singh Kushwaha, Jeremy Dhainaut

ChemComm
Chemical Communications

Accepted Manuscript

This article can be cited before page numbers have been issued, to do this please use: A. Sharma, U. Bhardwaj, M. Marinova, A. Da Costa, A. Ferri, S. Royer, H. S. Kushwaha and J. Dhainaut, *Chem. Commun.*, 2024, DOI: 10.1039/D4CC00463A.

ROYAL SOCIETY OF CHEMISTRY

rsc.li/chemcomm

View Article Online
DOI: 10.1039/D4CC00463A

COMMUNICATION

Borophene: A piezocatalyst for water remediation

Aditi Sharma,[a,b] Upasana Bhardwaj,[a] Maya Marinova,[c] Antonio Da Costa,[d] Anthony Ferri,[d] Sébastien Royer,[b] Himmat Singh Kushwaha[a*], Jérémy Dhainaut[b*]

Received 00th January 20xx,
Accepted 00th January 20xx

DOI: 10.1039/x0xx00000x

Borophene is an emerging two-dimensional material exhibiting exceptional piezocatalytic activity under the influence of ultrasonic vibrations, as exemplified herein by the decomposition of highly stable organic dyes in water. After 6 minutes of exposure, borophene sheets converted up to 92 percent of a mixture of dye molecules at room temperature.

Piezocatalysis is an emerging technique based on the piezoelectric effect of materials lacking a center of symmetry. Such materials deform themselves under the effect of mechanical vibrations, causing spontaneous polarization. Then, the free charge carriers inside the materials are separated through the induced piezopotential and can migrate to the surface to further engage in redox reactions.[1] The piezoelectricity produced by mechanical distortion in such materials has found widespread application in sensing, actuators, and high-voltage generators.[2]

Most known piezoelectric devices are comprised of bulk materials like ceramics and single crystals. The application of nanosized piezoelectric materials is newer.[1] Especially, two-dimensional materials have garnered a great deal of interest due to their high surface-to-volume ratio and exceptional electronic properties, which grant them with a greater potential for various applications such as energy storage, sensing, electronics, aerospace structures than their bulk form.[2] In 2014, it was discovered for the first time that MoS_2 nanosheets exhibit substantial piezoelectric properties.[3] After the development of 2D materials such as graphene,[4] silicene,[5] hexagonal boron nitride,[6] stanine, aluminum nitride sheet, phosphorene,[7] arsenene, molybdenum disulfide, and antimonene, 2D boron sheets known as borophene were unveiled.[8] Borophene has rich architectural diversity, exhibiting unique physical and chemical properties including- in-plane anisotropy, ultrahigh thermal conductance, superconductivity, high carrier mobility, presence of dirac fermions, and optical transparency.[9] Boron-related 2D compounds are distinguished from other 2D materials by their polymorphism,[10] *i.e.*, the capacity of boron to create multicenter bonding arrangements enabling the formation of a large variety of stable 2D phases. Especially, the β12 phase of borophene is anisotropic. Due to this, the unique character of boron-boron multicenter bonds has been elucidated theoretically, resulting in great bending flexibility and optimum strength along various orientations of the borophene. As a result, the findings suggest that borophene is a promising material, with potential applications as a piezocatalyst, among others.[11]

Initially, borophene was synthesized by chemical vapor deposition on a metal substrate.[12] However, this method produces limited amounts of borophene. For larger synthesis scales, a modified Hummer's method has been recently proposed.[11] The resulting two-dimensional material is easily deformable, and its flat surface gives a large area for capturing mechanical energy. Under ultrasonication, these nanosheets readily degrade organic pollutants, for instance organic dyes in water. By monitoring the reactive radicals produced during the piezocatalytic process, a degradation mechanism of organic dyes involving superoxide ($\bullet O_2^-$) and hydroxyl ($\bullet$OH) oxidant radicals is proposed.

The XRD pattern of the synthesized borophene sheets is depicted in Figure S1-a, and it matches well with the β-rhombohedral crystalline structure of boron (ICDD card no 00-031-0207).[13] The reduced peaks intensity may suggest that upon formation, the crystals grow following a preferential orientation.[14] Hence, to confirm the formation of borophene

[a] *Materials Research Centre, Malaviya National Institute of Technology Jaipur (MNITJ), India.*
[b] *Univ. Lille, CNRS, Centrale Lille, Univ. Artois, UMR 8181 - UCCS - Unité de Catalyse et Chimie du Solide, F-59000 Lille, France.*
[c] *Université de Lille, CNRS, INRA, Centrale Lille, Université Artois, FR 2638 – IMEC – Institut Michel-Eugène Chevreul, 59000 Lille, France.*
[d] *Univ. Artois, CNRS, Centrale Lille, Univ. Lille, UMR 8181, Unité de Catalyse et Chimie du Solide (UCCS), F-62300 Lens, France.*

Electronic Supplementary Information (ESI) available: Experimental protocols, additional characterization (XRD, Raman, XPS, AFM), oscilloscope measurements, additional catalytic data and scavenging experiments. See DOI: 10.1039/x0xx00000x

sheets, their raman spectrum is depicted in Figure S1-b. The improved Hummer's process produced borophene sheets with distinct Raman peaks which matches well with the boron appearing at 234 cm^{-1}, 379.15 cm^{-1}, 696 cm^{-1}, 911.05 cm^{-1}, 1062 cm^{-1} and 1155 cm^{-1}.[15] Borophene, unlike graphene, is anisotropic; as a result, its symmetry axes are not identical, resulting in multiple distinctive peaks.[11] High resolution XPS, as shown in Figure S1-c was further applied to evaluate the surface composition of borophene. As synthesized borophene displays three peaks in B 1s spectrum centered at 192.5, 189.1, and 187.7 eV, showing that B created three types of bonding structures. The principal component related to a B–B bond at 187.7 eV is comparable with the previously reported values for bulk B (187.3-187.9 eV),[16] while the peak attributed to the B–O bond in a boron-rich oxide, is located at 189.1 eV. The 192.5 eV signal appears to be related to the production of B_2O_3, indicating that borophene may be partially oxidized due to its large contact area.[17]

Representative BF-TEM and HR-TEM images together with a respectively SAED pattern and a fast Fourier Transform (FFT) pattern, respectively are presented in Figure 1a-b and their insets. These images were taken on the powder sample. A representative HAADF image in the cross-section is shown in Figure S2. The SAED pattern has been indexed and best matches with the [100] zone axis of β-rhombohedral boron structure (space group: R-3m (166) and a=10.9251(2) Å; b=10.9251(2) Å; c=23.8143(8) Å).[18] The thickness of the borophene sheets varies between approximately 5 nm and 15 nm as shown in Figure S3. These sheets have parallel atomic ridges and are crystalline. The interplanar distance measured (0.326 nm) from the cross-sectional HAADF image matches with the (300) plane of β_{12} borophene which agree with the TEM images.[19] Figure S3 shows atomic force microscopy (AFM) images depicting that the thickness of borophene stacked nanosheets is ranging from 2 to 15 nm, matching with TEM observations. Of note, the lateral dimensions of as-produced borophene can also be observed and are above 200 nm.

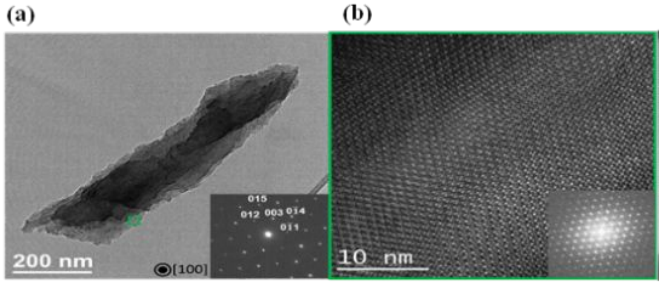

Figure 1. (a-b) BF-TEM and HR-TEM images with SAED and fast Fourier Transform (FFT) patterns, respectively.

A PFM approach was used to probe the piezoelectric properties of borophene nanosheets at the nanoscale. When AC driving voltage is applied to the sample via the AFM tip, the ensuing mechanical deformation of the material is induced due to the converse piezoelectric effect.[20] The as-grown out-of-plane (OP) and in-plane (IP) amplitude piezoresponse patterns measured over the surface of the borophene sample are presented in Figures 2b and c, respectively, simultaneously recorded with the topography in Figure 2a. Due to the contact mode used, the AFM image appears blurry. Nonetheless, strong piezoelectric response is detected along both OP and IP direction, as revealed by the bright contrasts. By superimposing a continuous DC bias voltage (voltage pulse bias ramps from -10 V to +10 V) on the intermittent AC signal, amplitude piezoresponse loops can be recorded. As seen in Figure 2d, a well-defined butterfly-shaped loop is obtained, evidencing clear piezoelectric behavior in borophene,[21] in agreement with amplitude PFM pattern in Figure 2b. As a remark, the poor quality of the AFM topographic image presented in Figure 2a is mainly due to the contact mode required for simultaneously recording the topographic and piezoresponse signals.

Figure S4a shows digital scanning oscilloscope (DSO) measurements of the open circuit voltage response of mechanically stressed borophene sheets. Under bending conditions, the maximum voltage reaches up to 0.078 V, and it reaches 0.18 V when pressure was exerted by manual tapping. When pressure is imposed onto the borophene sheets, the induced piezopotential generates positive impulses, and when pressure is removed from the borophene sheets, the induced piezopotential generates negative impulses. The piezoelectric effect was not observed in the absence of vibrations, implying that no pressure was applied to or removed from the borophene sheets.[22] Figure S4b shows the piezo current response for the borophene sheets. It has good charge separation efficiency and high electron mobility.

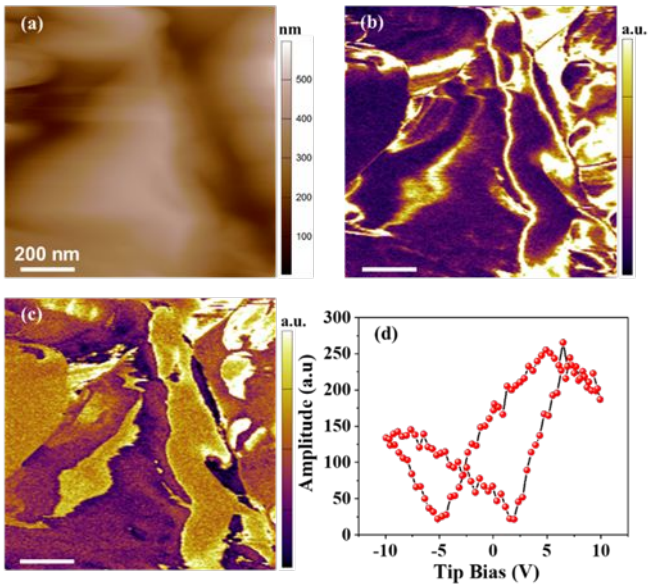

Figure 2. (a) AFM morphology, (b) amplitude OP-PFM, and (c) amplitude IP-PFM images simultaneously recorded on the borophene surface, and (d) characteristic amplitude piezoresponse loop recorded on borophene nanosheets.

Borophene was applied to the degradation of organic pollutants, and the piezocatalytic results are depicted in Figure 3a-b. In the case of methylene blue (MB), the absorbance peak at 668 nm decreases significantly from 6 minutes of ultrasonic

vibrations (Figure S5-a). Figure S5-b shows the degradation of a mixture of dyes (rhodamine b, MB, methyl orange, and rose Bengal) following 6 minutes of exposure time under ultrasonic vibrations. It has been showed that 92% of all dye molecules were readily deteriorated at room temperature and without addition of an oxidant as typically done in photocatalysis (H_2O_2, persulfates).[23] The relating decomposition ratios are summed up in Figure S5-c. MB and a mixture of dyes were degraded up to 97%, and 92% after 6 minutes. Figure 3a depicts the degradation efficiency curve, which was computed by subtracting the starting concentration from the concentration obtained after treatment. Importantly, no degradation occurs when only ultrasonic vibrations or borophene are applied to organic dyes. The corresponding degradation rate constants were determined by fitting the empirical observations to the pseudo-first order kinetic rate equation (-ln kt= C/C_0), as shown in Figure 3b. Under ultrasonication, the degradation rate constant of MB is k = -0.4495 min^{-1}, whereas the rate constant for the mixture of dyes is k = -0.60675 min^{-1}. In addition, the recyclability of borophene for degrading MB was examined without pre-treatment. The degradation efficiency was slightly reduced from the sixth cycle (-3% compared to the initial rate), confirming the robustness of borophene as a piezocatalyst for long-term applications (Figure S6-a). The structural stability of borophene nanosheets also provides solid proofs that the degradation of MB is caused by the piezocatalytic effect of borophene, rather than by any direct chemical reaction between borophene and organic dye. However, as shown in Figure S6-b and -c, very few boron oxide (B_2O_3) is formed after six cycles (36 minutes total exposure time). Table S1 finally compares different piezocatalytic systems applied to MB degradation, highlighting the superior performances of borophene.

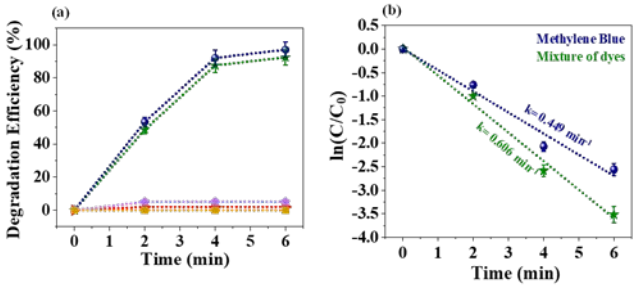

Figure 3. (a) Degradation efficiency of borophene (blue: methylene blue + borophene + ultrasounds, green: mixture of dyes + borophene + ultrasounds, purple: methylene blue + borophene, red: mixture of dyes + borophene, orange: methylene blue + ultrasounds), (b) kinetic order curves.

The scavenger study was carried out to investigate the involvement of active radical species in the breakdown of MB by borophene sheets via a piezocatalytic mechanism. Isopropyl alcohol (IPA) scavenged hydroxy radicals (OH•), para-benzoquinone (BQ) scavenged superoxide ($•O_2^-$), and ethylenediaminetetraacetate (EDTA) scavenged holes (h^+). These scavengers were coupled with borophene sheets and the MB solution. As demonstrated in Figure S7, the breakdown efficiency of MB molecules was dramatically reduced when isopropanol alcohol (IPA) and benzoquinone (BQ) were added to the MB aqueous solution. However, when disodium ethylene diamine tetra-acetate dehydrates (EDTA-2Na) was added to the reaction solution, only a minor decrease in degradation was detected. The findings indicate that the •OH and $•O_2^-$ radicals were generated and served as the primary reactive species in the piezocatalytic process.[24] Throughout the piezocatalytic process, fluorescence spectroscopy was employed to detect the formation of hydroxyl radicals (•OH) as they rapidly interact with terephthalic acid to form 2-hydroxyterephthalic acid, a highly fluorescent drug with a signal at 425 nm under 315 nm excitation.[25] As observed in Figure 4a, under ultrasonic irradiation borophene produces a consequent amount of hydroxyl radicals which are one of the main active species in liquid-phase advanced oxidation processes. Furthermore, the degradation of nitro blue tetrazolium chloride, which is a scavenger for super oxide radicals ($•O_2^-$), was carried out under the same conditions as dyes degradation.[8] As illustrated in Figure 4b, its degradation shows consequent formation of $•O_2^-$.

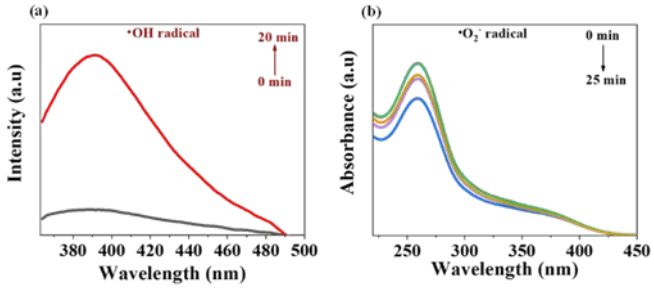

Figure 4. (a) Photoluminescence spectra for the detection of $OH^·$ radicals by using terephthalic acid, (b) Degradation of nitroblue tetrazolium (NBT) under the piezocatalytic effect to confirm the production of super oxide radical ($•O_2^-$).

Based on the above findings, a potential piezocatalytic mechanism interpretation is proposed in Figure S9. Initially, bound charges on the piezoelectric material's surface are in equilibrium with screening charges, resulting in an electrically neutral material.[26] Due to compressive stress caused by the piezoelectric action, the amplitude of polarization will be lowered. This, in turn, can cause charge carrier redistribution and the release of extra screening charges from the surface. As a result, the surplus charges disperse into solution and become free charges, combining with water molecules to generate reactive species like •OH and $•O_2^-$.[27] When the mechanical stress is imposed at its maximum level, the polarized charges will be minimized. The additional screening charges will continue to be released until the material attains new electrostatic balance.[28] When the applied stress is released, then the newly formed electrostatic equilibria will break again, increasing the polarization. The charges will thus be adsorbed from the surroundings to balance the bound charges caused by piezoelectric effect. In a similar manner to forward loading, the redox reactions at the solid-liquid interface will not last long due to the depletion of the surface charge. The free charges (e^- and h^+) that were spent by redox reactions can be produced again

thermally by the mechanical energy (ultrasonic vibrations), producing the apparent piezocatalytic effect. The main reactions that occur in the degradation mechanism are depicted in equations (1-4):

$$\text{borophene + mechanical stress} \rightarrow \text{borophene } (e^- + h^+) \quad (1)$$

$$O_2 + e^- \rightarrow \bullet O_2^- \quad (2)$$

$$H_2O + h^+ \rightarrow \bullet OH \quad (3)$$

$$\bullet O_2^- / \bullet OH + \text{pollutants} \rightarrow \text{degraded products} \quad (4)$$

In conclusion, this paper describes the synthesis of borophene nanosheets, as well as their characterization. Especially, the formation of a piezo-potential within the borophene nanosheets under the mechanical stress was measured to be ~ 0.2 V. Utilizing ultrasonic vibration energy, the piezocatalytic ability of borophene nanosheets to decompose single and mixture of organic dyes has been investigated. Under these conditions, borophene nanosheets efficiently degrade all types of dye molecules. Hydroxyl (•OH) and superoxide (•O2-) radicals are the primary oxidizing species that are produced from polarized electric charges. Our work will encourage additional research in the fields of piezocatalysis over borophene-based materials, especially in the field of water remediation.

Author Contributions

H.S.K., J.D. and S.R. conceived and designed the project. A.S. prepared the borophene, conducted most characterization, and did all catalytic tests. U.B. measured piezo potential and piezo current response with DSO. M.M. conducted HR-TEM observations, analysed and discussed HR-TEM data. A.D.C conducted PFM measurements. A.F. analysed and discussed the PFM data. A.S., J.D., H.S.K., and S.R. analysed all other data. A.S. wrote the original manuscript. All authors discussed the results and commented on the manuscript.

Conflicts of interest

There are no conflicts to declare.

Notes and references

1 J. Li, S. Chen, W. Liu, R. Fu, S. Tu, Y. Zhao, L. Dong, B. Yan, Y. Gu, *J. Phys. Chem. C* 2019, **123**, 11378.

2 H. Cui, X. Zhang, D. Chen, *Appl. Phys. A Mater. Sci. Process.* 2018, **124**, 636.

3 W. Wu, L. Wang, Y. Li, F. Zhang, L. Lin, S. Niu, D. Chenet, X. Zhang, Y. Hao, T. F. Heinz, J. Hone, Z. L. Wang, *Nature* 2014, **514**, 470.

4 A. A. Balandin, *Nat. Mater.* 2011, **10**, 569.

5 H. Dai, P. Xiao, Q. Lou, *Phys. Status Solidi A* 2011, **208**, 1714.

6 J. Dauber, A. A. Sagade, M. Oellers, K. Watanabe, T. Taniguchi, D. Neumaier, C. Stampfer, *Appl. Phys. Lett.* 2015, **106**, 193501.

7 S. Zhang, S. Guo, Z. Chen, Y. Wang, H. Gao, J. Gómez-Herrero, P. Ares, F. Zamora, Z. Zhu, H. Zeng, *Chem. Soc. Rev.* 2018, **47**, 982.

8 Z. A. Piazza, H. S. Hu, W. L. Li, Y. F. Zhao, J. Li, L. S. Wang, *Nat. Commun.* 2014, **5**, 3113.

9 S. Y. Xie, Y. Wang, X. Bin Li, *Adv. Mater.* 2019, **31**, 1900392; A. J. Mannix, X. F. Zhou, B. Kiraly, J. D. Wood, D. Alducin, B. D. Myers, X. Liu, B. L. Fisher, U. Santiago, J. R. Guest, M. J. Yacaman, A. Ponce, A. R. Oganov, M. C. Hersam, N. P. Guisinger, *Science* 2015, **350**, 1513; B. Feng, J. Zhang, Q. Zhong, W. Li, S. Li, H. Li, P. Cheng, S. Meng, L. Chen, K. Wu, *Nat. Chem.* 2016, **8**, 563; A. J. Mannix, Z. Zhang, N. P. Guisinger, B. I. Yakobson, M. C. Hersam, *Nat. Nanotechnol.* 2018, **13**, 444.

10 Y. Jiao, F. Ma, J. Bell, A. Bilic, A. Du, *Angew. Chem. Int. Ed.* 2016, **55**, 10292; T. Kondo, *Sci. Technol. Adv. Mater.* 2017, **18**, 780; Z. Zhang, E. S. Penev, B. I. Yakobson, *Chem. Soc. Rev.* 2017, **46**, 6746.

11 C. Hou, G. Tai, Y. Liu, X. Liu, *Nano Res.* 2022, **15**, 2537; Z. Zhang, E. S. Penev, B. I. Yakobson, *Chem. Soc. Rev.* 2017, **46**, 6746; P. Ranjan, T. K. Sahu, R. Bhushan, S. S. R. K. C. Yamijala, D. J. Late, P. Kumar, A. Vinu, *Adv. Mater.* 2019, **31**, 1900353; P. Ranjan, J. M. Lee, P. Kumar, A. Vinu, *Adv. Mater.* 2020, **32**, 2000531.

12 M. Ou, X. Wang, L. Yu, C. Liu, W. Tao, X. Ji, L. Mei, *Adv. Sci.* 2021, **8**, 2001801; Y. Liu, G. Tai, C. Hou, Z. Wu, X. Liang, *ACS Appl. Mater. Interfaces* 2023, **15**, 14566.

13 N. Taşaltın, S. Güllülü, S. Karakuş, *Inorg. Chem. Commun.* 2022, **136**, 109150.

14 F. Zhang, L. She, C. Jia, X. He, Q. Li, J. Sun, Z. Lei, Z. H. Liu, *RSC Adv.* 2020, **10**, 27532.

15 Q. Fan, C. Choi, C. Yan, Y. Liu, J. Qiu, S. Hong, Y. Jung, Z. Sun, *Chem. Commun.* 2019, **55**, 4246.

16 T. T. Xu, J. G. Zheng, N. Wu, A. W. Nicholls, J. R. Roth, D. A. Dikin, R. S. Ruoff, *Nano Lett.* 2004, **4**, 963.

17 H. Li, L. Jing, W. Liu, J. Lin, R. Y. Tay, S. H. Tsang, E. H. T. Teo, *ACS Nano* 2018, **12**, 1262.

18 B. Callmer, *Acta Crystallogr. Sect. B* 1977, **33**, 1951.

19 D. Ma, R. Wang, J. Zhao, Q. Chen, L. Wu, D. Li, L. Su, X. Jiang, Z. Luo, Y. Ge, J. Li, Y. Zhang, H. Zhang, *Nanoscale* 2020, **12**, 5313; C. Taşaltın, T. A. Türkmen, N. Taşaltın, S. Karakuş, *J. Mater. Sci. Mater. Electron.* 2021, **32**, 10750.

20 A. Gruverman, M. Alexe, D. Meier, *Nature Commun.*, 2019, **10**. 1661.

21 Q. Tang, J. Wu, D. Kim, C. Franco, A. Terzopoulou, A. Veciana, J. Puigmartí-Luis, X. Z. Chen, B. J. Nelson, S. Pané, *Adv. Funct. Mater.* 2022, **32**, 2202180; E. Lin, N. Qin, J. Wu, B. Yuan, Z. Kang, D. Bao, *ACS Appl. Mater. Interfaces* 2020, **12**, 14005.

22 A. Sharma, U. Bhardwaj, H. S. Kushwaha, *Mater. Adv.* 2021, **2**, 2649; A. Sharma, U. Bhardwaj, D. Jain, H. S. Kushwaha, ACS Omega 2022, **7**, 7595.

23 D. Ma, H. Yi, C. Lai, X. Liu, X. Huo, Z. An, L. Li, Y. Fu, B. Li, M. Zhang, L. Qin, S. Liu, L. Yang, *Chemosphere* 2021, **275**, 130104.

24 F. Bößl, T. P. Comyn, P. I. Cowin, F. R. García-García, I. Tudela, *Chem. Eng. J. Adv.* 2021, **7**, 100133.

25 A. Sharma, U. Bhardwaj, H. S. Kushwaha, *Catal. Sci. Technol.* 2022, **12**, 812.

26 O. Copie, N. Chevalier, G. Le Rhun, C. L. Rountree, D. Martinotti, S. Gonzalez, C. Mathieu, O. Renault, N. Barrett, *ACS Appl. Mater. Interfaces* 2017, **9**, 29311.

27 J. Wu, W. Mao, Z. Wu, X. Xu, H. You, A. Xue, Y. Jia, *Nanoscale* 2016, *8*, 7343–7350; H. Lei, M. Wu, Y. Liu, F. Mo, J. Chen, S. Ji, Y. Zou, X. Dong, *Chinese Chem. Lett.* 2021, **32**, 2317.

28 Y. Zi, L. Lin, J. Wang, S. Wang, J. Chen, X. Fan, P. K. Yang, F. Yi, Z. L. Wang, *Adv. Mater.* 2015, **27**, 2340.